PHYSICAL REVIEW B VOLUME 12, NUMBER 9 1 NOVEMBER 1975

"Diffraction" and microscopy in solids and liquids by NMR*

P. Mansfield and P. K. Grannell†
Department of Physics, University of Nottingham, Nottingham NG7 2RD, England
(Received 29 July 1974)

A new approach to the study of structure in solids and liquids by pulsed NMR is described. Either multiple-pulse line-narrowing sequences or single pulses, together with an applied linear magnetic field gradient are used. The theoretical analysis highlights the analogy with plane-wave scattering in optics and is illustrated experimentally with examples of diffraction by ordered and disordered systems and image formation or microscopy. The factors affecting the resolution of the technique are discussed, and the problems of reconstructing micrographs from their projections considered.

I. INTRODUCTION

The study of internuclear spacings in solids by NMR has traditionally relied upon the dipole-dipole interaction and its effect on line shape and second moment in order to estimate intramolecular distances. Although all information on the unit cell is contained in the dipolar lattice sums, there is no direct way of obtaining the lattice structure from the free-induction decay (FID) or from the dipolar line shape of a solid. In general, one needs a hypothetical model of the structure being determined, so that the theoretical predictions for the second moment or for the line shape may be compared with results obtained experimentally. This all comes about because a particular lattice site is not uniquely determined magnetically and hence is not uniquely identifiable in the frequency spectrum.

Recently,[1,2] we introduced a new method for the determination of spatial structures in solids, which relies on NMR diffraction effects, in which identification of the lattice sites in the frequency spectrum is obtained by applying a linear magnetic field gradient to the sample. Lauterbur[3] has independently introduced a similar method for studying the localized liquid regions in biological systems. The usual effect of a gradient is to produce a FID which, through a Fourier transform, reflects the bulk shape of the material, assumed to be a *continuous* distribution of spins. This has been discussed by Gabillard[4,5] and others.[6-8]

Of course, in a solid, the spins are actually distributed in a *discrete* manner at atomic sites. One reason that this discrete nature is not apparent in the observed FID signals is the large dipole-dipole broadening in solids. However, this may be removed by using one of the recently developed multiple-pulse sequences,[9-11] or a derivative to be described here. Self-diffusion is another broadening mechanism which may be made arbitrarily small by lowering the sample temperature.

The effect of a discrete structure may be illustrated by considering a model one-dimensional regular lattice: the NMR spectrum of a number of uniformly spaced layers of liquid-like material ("Vaseline" grease) containing resonant nuclei is split by the application of a field gradient into a "grating" spectrum. The nuclear transient response from such a regular array of resonant spins resembles the well-known intensity distribution resulting from the diffraction of monochromatic light at a grating. Figure 5(b) demonstrates the diffraction effect for seven equally spaced slices. The details of this experiment are given in Sec. III D 2.

The analogy between the phase difference obtained (a) from the different path lengths to the various grating slits in the optical experiment, and (b) from the different free-precessional frequencies associated with the various nuclear positions in the linear field gradient of the NMR experiment, have led us to call this phenomenon NMR "diffraction."

In this paper, which is an amplification and extension of our earlier letter,[1] we show that there is a formal analogy between the familiar scattering of a plane electromagnetic wave by a regular lattice and the "scattering" of the Green's function which describes the spin response in the magnetic field gradient. This is treated in Secs. II and III. In Sec. IV we show that NMR diffraction may also be applied to partially disordered systems. The factors affecting the limits to spatial resolution common to both diffraction and microscopy experiments are discussed in Sec. V. Finally, in Sec. VI the diffraction theory is extended to continuously distributed spin systems and the optical analogy of microscopy developed. Some experimental results are also given which include an example of a one-dimensional spin-density distribution or projection recorded in a physiological specimen *in vivo*, and a two-dimensional reconstructed image or micrograph.

II. THEORY

A. General formalism

The transverse NMR response signal in the rotating reference frame may be represented by the retarded Green's function[12]

$$\Gamma^r(t)=\lim_{\epsilon\to 0}\sum_i \Theta(t)\,\frac{\langle[I_{+i}(t),I_{-i}(0)]\rangle\, e^{-\epsilon t}}{\sum_i\langle[I_{+i},I_{-i}]\rangle}\,, \tag{1}$$

where the step function

$$\Theta(t)=\begin{cases}0 & \text{for } t\le 0\\ 1 & \text{for } t>0\end{cases}. \tag{2}$$

The time development of the spin-displacement operators $I_\pm$ is given by

$$I_\pm(t)=e^{iHt}I_\pm e^{-iHt}\,, \tag{3}$$

where the Hamiltonian, with $\hbar=1$, is

$$H=H_0+H_1\,, \tag{4}$$

and comprises the Zeeman term $H_0=-\Delta\omega_0\sum_i I_{zi}$ and an interacting or perturbing term H_1.

We shall consider a set of N noninteracting nuclei with spin number I, the total Green's function of which is just N times the single-particle Green's function $G^r(t)$. Differentiating Eq. (1) leads to the exact equation of motion[13]

$$G^r(t)=G_0^r(t)+\int_{-\infty}^{+\infty} G_0^r(t')G_1^r(t-t')\,dt'\,, \tag{5}$$

where $G_0^r(t)$ is the unperturbed Green's function evolving under the influence of H_0 alone, and

$$G_1^r(t)=\lim_{\epsilon\to 0}\Theta(t)\,\frac{\langle[[H,I_+(t)],I_-(0)]\rangle}{\langle[I_+,I_-]\rangle}\,e^{-\epsilon t} \tag{6}$$

is a higher-order Green's function involving the total Hamiltonian H.

Equation (5) is the Green's-function scattering equation and has its counterpart in the usual theory of plane-wave scattering.[14] We shall develop the analogy further.

B. Linear field gradient perturbation

The interaction of spins with the magnetic field gradient tensor $\vec{\mathcal{G}}$ may be written generally as[15]

$$H_1=\gamma\vec{r}\cdot\vec{\mathcal{G}}\cdot\vec{I}=\gamma\vec{B}\cdot\vec{I}\,. \tag{7}$$

However, if linear gradients

$$\begin{aligned}\mathcal{G}_{xz}&=\frac{\partial}{\partial x}B_z\,,\\ \mathcal{G}_{yz}&=\frac{\partial}{\partial y}B_z\,,\\ \mathcal{G}_{zz}&=\frac{\partial}{\partial z}B_z\end{aligned} \tag{8}$$

only are applied, all other tensor components being zero, then we may define a vector gradient

$$\vec{G}=\hat{i}\,\mathcal{G}_{xz}+\hat{j}\,\mathcal{G}_{yz}+\hat{k}\,\mathcal{G}_{zz}\,, \tag{9}$$

which completely specifies the interaction as follows:

$$H_1=\gamma(\vec{r}\cdot\vec{G})I_z\,. \tag{10}$$

C. Fictitious wave

The Zeeman interaction as well as the gradient interaction are assumed to arise from a scattering process. In order to view the interactions this way, it is necessary to regard the Zeeman term itself as arising from the interaction of a spin with the real field gradient $\vec{G}$.

We represent the scattering process diagrammatically in Fig. 1(a) by a fictitious wave originating at the source S, at position $\vec{r}_0$ from 0. This wave is scattered from $\vec{p}_0$ to $\vec{p}_0'$ through an angle Θ to a point D by the gradient interaction with a spin at 0 with position $\vec{s}$ from the origin 0′, where the initial "momentum" $\vec{p}_0=\gamma\vec{G}_0 t$. As is customary with plane-wave scattering, we take $\vec{p}_0=p_0\hat{r}_0$ and $\vec{p}_0'=p_0\hat{r}_0'$, where $\hat{r}_0$ and $\hat{r}_0'$ are unit vectors along $\vec{r}_0$ and $\vec{r}_0'$, respectively.

The phase of our wave accumulated in going from S to D is

$$\vec{p}_0\cdot\vec{r}_0+\vec{p}_0'\cdot\vec{r}_0'=\gamma G_0(r_0+r_0')t=\gamma t\,\vec{G}\cdot\vec{s}=\Delta\omega_0 t\,, \tag{11}$$

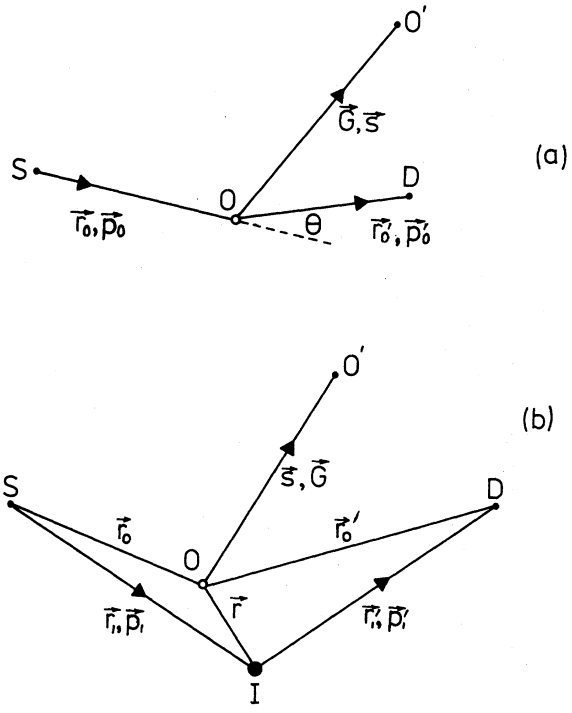

FIG. 1. Fictitious wave diagrams representing the scattering of Green's functions.

subject to the constraint that

$$G = G_0\sqrt{2}\,(1-\cos\Theta)^{1/2}. \tag{12}$$

The applied field gradient $\vec{G} = G\hat{s}$, where $\hat{s}$ is a unit vector along $\vec{s}$.

1. Scattering at $\vec{r}$

Again we consider a fictitious wave originating at source S which is scattered from $\vec{p}_1$ to $\vec{p}_1'$ by the gradient interaction with a spin I placed at position $\vec{r}$ from 0 [see Fig. 1(b)]. In this case, we take $\vec{p}_1 = p_0\hat{r}_1$ and $\vec{p}_1' = p_0\hat{r}_1'$. The Green's function, Eq. (5), along the new path SID becomes, therefore,

$$G^r(\vec{p}_1, \vec{p}_1') = e^{i(\vec{p}_1\cdot\vec{r}_1 + \vec{p}_1'\cdot\vec{r}_1')} \approx e^{i(\vec{p}_0\cdot\vec{r}_0 + \vec{p}_0'\cdot\vec{r}_0')}\, e^{i(\vec{p}_1 - \vec{p}_1')\cdot\vec{r}}, \tag{13}$$

for $\hat{r}_1 = \hat{r}_0$ and $\hat{r}_1' = \hat{r}_0'$, that is, for $\vec{r}_0$, $\vec{r}_0'$ large. This corresponds to the parallel-ray approximation in optics. Equation (13) is the complex response signal of a single spin in a field gradient.

If we were to consider two spins, the second of which be placed at 0 in Fig. 1(b), then the sum of the amplitudes of the scattered fictitious waves corresponds exactly to that obtained from the point-diffraction theory in optics (apart from common factors of $1/r$) when the source and image points are sufficiently far from the scattering center, that is to say, in the parallel-ray approximation. Also, the condition for constructive or destructive interference is identical.

III. DIFFRACTION FROM STATIC NONINTERACTING SPINS

A. General

We consider a set of static noninteracting spins in an orthorhombic lattice with unit-cell dimensions a, b, c. The displacement vector $\vec{r}_{lmn}(k)$ from the origin of the kth spin site in the (l, m, n)th unit cell (l, m, n integer) is given by

$$\vec{r}_{lmn}(k) = (l+u_k)\vec{a} + (m+v_k)\vec{b} + (n+w_k)\vec{c}, \tag{14}$$

where $\vec{a} = a\hat{i}$, etc., and u_k, v_k, w_k are fractions of the primitive-cell dimensions.

For a semidiscrete spin distribution in a uniform magnetic field gradient $\vec{G}$, in which the spins are distributed with a density of $\rho(\vec{r})$ over a range $\Delta x, \Delta y, \Delta z$ from the position $\vec{r} = \vec{r}_{lmn}(k) + \vec{r}'$, where $\vec{r}'$ is a continuous variable, we obtain for the FID function of the system at resonance [see Eq. (13)],

$$S(\vec{p}) = \mathrm{Re}\sum_{l,m,n,k}\int_{(l+u_k)a}^{(l+u_k)a+\Delta x}\int_{(m+v_k)b}^{(m+v_k)b+\Delta y}\int_{(n+w_k)c}^{(n+w_k)c+\Delta z}\rho(\vec{r})e^{i\vec{p}\cdot\vec{r}}\,d\vec{r}', \tag{15}$$

where $\vec{p} = \vec{p}_1 - \vec{p}_1' = \gamma\vec{G}t$, in which γ is the nuclear magnetogyric ratio and t is the elapsed time.

For a set of point spins, as in a crystal lattice, Eq. (15) reduces to

$$S = \mathrm{Re}\sum_{l,m,n} a_{lmn}\exp[2\pi i(le+mf+ng)] \times\sum_k f_k\exp[2\pi i(u_k e + v_k f + w_k g)], \tag{16}$$

where $e = \gamma t a G_x/2\pi = a p_x/2\pi$, etc., and $a_{lmn} = 0, 1$. The term involving the summation over k corresponds to signal contributions within the unit cell, and is equivalent to the geometrical structure factor S_k in electron or neutron scattering. In our case, the scattering cross section $f_k = 0, 1$. Unlike ordinary x-ray scattering, NMR scattering is in principle selective, since only resonant spins contribute to the signal, nonresonant spins having $f_k = 0$. This is an important point in the study of protons in solids which are effectively transparent to x rays.

Also, since we observe the amplitude of the scattered Green's function rather than the intensity of a scattered wave as in x rays, there is no phase problem. The phase of the "carrier wave" is implicit in the NMR diffraction pattern, provided phase-sensitive demodulation of the signal is used. It is clear that the dimensionless quantities e, f, g correspond to the lattice Miller indices at appropriate times t.

B. Solids

The point-spin formula Eq. (16) shows that in a cubic lattice with $\vec{G}$ along the [001] axis, observation of first-order diffraction requires $g = 1$. For protons with a typical lattice spacing, $c = 3$ Å and a maximum feasible gradient $G_z = 10^3$ G cm^{-1}, the diffraction peak would occur at 8 sec from the time origin. Thus, in order to observe this signal, an intrinsic narrowed linewidth of about 0.1 Hz would be required. By employing one of the recently developed multiple-pulse sequences,[9-11] or a suitable modification described below, the principal broadening terms in a solid, that is to say, the dipolar and chemical-shift interactions, may be artificially reduced to a very high degree, while at the same time leaving the spin-field gra-

dient interaction only slightly reduced. This can be achieved by applying a modified compensated reflection-symmetry cycle, designed to remove dipolar and chemical-shift terms, while at the same time appropriately reversing the linear-field-gradient direction. Such a sequence is, in the pulse-timing representation,

$$P_{-y} - [\tau(+) - P_x - \tau(+) - P_y - 2\tau(+) - P_y - \tau(+) - P_x - 2\tau(-) - P_x - \tau(+) - P_y - 2\tau(-) - P_y - \tau(+) - P_x - \tau(+)]_N ,$$

where $\tau(\pm)$ indicates the sense of the field gradient applied during the delay τ. To date, the best line-narrowing achieved in a single crystal of CaF_2 is about 20 Hz,[16] using standard multiple-pulse methods. Thus practical realization of crystallography by NMR diffraction is some way off. In addition, the application of large field gradients degrades the line-narrowing efficiency in the present-day cycles,[11] but this effect may be reduced by using samples of very small diameter so that the total static-field variation over the sample is kept within a reasonable limit of about 1.0 G.

At this point we may ask what field gradient would be necessary to observe first-order diffraction in a solid excited by a single 90° rf pulse? Again; if we take $c = 3$ Å and insist that the diffraction peak be observed within about $2T_2 \sim 100$ μsec, we find that $G_z = 10^8$ G cm^{-1}!

1. Biological systems

NMR diffraction could be useful at the macroscopic level in biophysical and other system, if the material has an approximately regular structure. When there is little motion, e.g., in frozen cell membranes or filamentary or fibrous structures, some artificial line-narrowing would certainly be required. As an approximation to such a system, we consider a uniform one-dimensional lattice of lattice constant c, which comprises $N+1$ flat slabs of thickness Δz containing uniformly distributed spins, Fig. (2). For this model, Eq. (15) gives for the normalized transient signal

$$S(p_z) = \left(\exp[i p_z (\Delta z + Nc)/2] \times \frac{\sin\beta}{\beta} \frac{\sin[p_z c(N+1)/2]}{(N+1)\sin(p_z c/2)} \right), \qquad (17)$$

where $\beta = \frac{1}{2}\gamma G_z t \Delta z$. This result is similar to the classical diffraction-grating formula. The $\sin\beta/\beta$ term represents the signal coming from one plate of thickness Δz, and corresponds to the results obtained by Gabillard,[4,5] Bradford *et al.*,[6] and Carr and Purcell[7] in the interference limit of continuously distributed spins.

Although we have stressed here the regularity of the structure to be studied, we shall see in Secs. IV and VI that the formalism presented is quite general and allows the analysis and study of *nonregular* structures.

C. Liquids

1. Babinet's principle

In this section we shall ignore the broadening effect caused by translational self-diffusion. This, together with its effect on spatial resolution, will be fully discussed in Sec. V.

Since the random isotropic thermal motion in a mobile liquid automatically averages the dipolar interaction to zero, there is, in general, no need to employ multiple-pulse techniques as for solids. Experimentally, observation of the FID following a single 90° rf pulse is all that is required. Of course, with a liquid, it is harder to define or recognize a rigid lattice. However, if we imagine a rigid lattice of solid spheres of spins, completely immersed in an isotropic homogeneous fluid of noninteracting spins of constant density ρ_0, then it is clear that the response of such a system to a single 90° pulse is

$$S(\vec{p}) = \mathrm{Re} \sum_{l,m,n} \int_{la}^{la+\Delta x} \int_{mb}^{mb+\Delta y} \int_{nc}^{nc+\Delta z} [\rho_0 - \rho(\vec{r})] \times e^{i\vec{p}\cdot\vec{r}}\, d\vec{r}' , \qquad (18)$$

where we assume that, because of its shorter-lived transverse signal, the solid contribution to the signal, $\rho(\vec{r})$, is not observed. Thus, instead of observing the diffraction from the solid spheres directly, a complementary pattern from the liq-

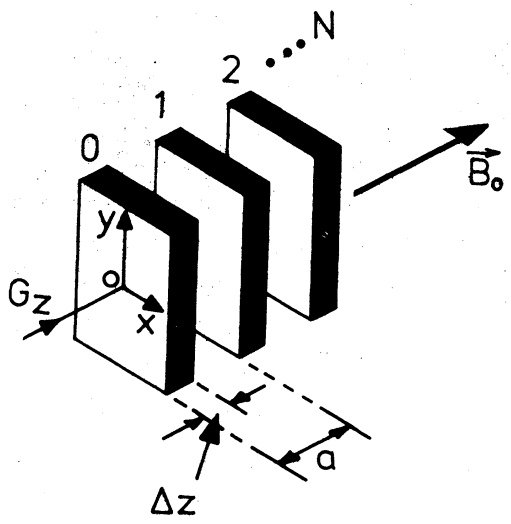

FIG. 2. Model of a one-dimensional lattice.

uid is observed. This complementary effect has its counterpart in optical diffraction, where it is known as Babinet's principle. Of course, if both solid and liquid signals were observed, and if the spins in each component were uniformly and homogeneously distributed with constant density, then a signal reflecting the bulk shape of the sample would be observed. That is to say, the sum of the narrowed absorption spectra from a solid and that of its complement obtained by immersion in a liquid, should be constant within the over-all lineshape.

Although we have so far discussed regular solid arrays immersed in a liquid, it is clear from the foregoing theory that Babinet's principle should hold whatever the solid spin distribution. This can easily be shown from Eq. (16) in the limit of a continuous, nondiscrete rather than semidiscrete, material. The application of Babinet's principle to continuous systems is discussed in Sec. VI of this paper.

It would thus appear that the difficult problem of removing the dipolar interaction in solids in order to study spatial spin distributions, and hence structure, may be obviated by immersing the solid in a suitable liquid and then studying the liquid signal. One could no doubt think of artificial systems to achieve this, but of course, most biological materials approximate well to such an immersed system with something like (80–90)% water surrounding between (10–20)% solid material. A physiological example of such a system would be bone surrounded by normal flesh, which approximates well to a solid immersed in a liquid, *vide infra*. Of course, in such biological systems, one might well be interested in the density variations *within* the solid as well as the *external* shape of the solid, indeed, whether there be solid material at all or simply a hole! In this case one would have to study the material using both single- and multiple-pulse excitations and then by Babinet's principle subtract off the true liquid part of the distribution to reveal the solid spin-density distribution.

The subject of nonregular density distributions will be discussed more fully in Secs. IV and VI.

2. *Spin-lattice relaxation time mapping*

The formalism as developed in Eq. (15) can easily be extended to systems with macroscopic regions with localized spin-lattice relaxation times $T_1(\vec{r})$. In this case, the localized equilibrium scattering cross section, which is proportional to spin density $\rho(\vec{r})$ and the local spin populations will, if perturbed from equilibrium, reflect variations of T_1 throughout the sample. For example, if the spin system is initially prepared by population inversion (an initial 180° rf pulse), subsequent inspection after a time t by the procedures discussed above will yield an effective spin density

$$\rho(\vec{r}, t) = \rho(\vec{r})(1 - 2e^{-t/T_1(\vec{r})}) . \tag{19}$$

Further experiments in which t is varied will allow the spin-lattice relaxation times $T_1(\vec{r})$ to be mapped.

D. Experimental results for regular arrays of solids and liquids

1. *Solids*

As a preliminary test of our results [Eqs. (15) and (17)], we have applied the $[\![1, 3, 2; 1, \bar{3}, 2]\!]$ multiple-pulse line-narrowing sequence[10] with $\tau = 6.4$ μsec to protons in model one-dimensional lattices comprising equally spaced plates of solid camphor. In these experiments, the field gradient is kept constant so that the chemical-shift terms, which are rather small for protons, are retained in the average Hamiltonian. However, the spatial resolution achieved is governed by much larger deviations from field-gradient uniformity due to the coil design.[17] The important point is not so much the resolution, which at present corresponds to 0.5 mm, but that temporal coherence of the first-order diffraction peak is restored due to removal of the dipole-dipole interaction in a solid.

Figure 3(a) shows the transient signal from a three-layer camphor sample with zero applied field gradient recorded at 9.0 MHz. The receiver coil was cylindrical with a 9.5-mm-diam access. The nuclear signal from camphor in the absence of artificial line-narrowing decays with $T_2 \sim 44$ μsec. Figure 3(b) shows the transient signal as for Fig. 3(a), but with an applied field gradient $G_z = 0.77$ Gcm^{-1}. Note the first-order diffraction peak. Figure 3(c) shows the narrowed transient signal from a five-layer camphor sample under the same conditions. A first-order diffraction peak is observed here also. All these data were recorded at room temperature and off resonance, to facilitate Fourier transformation.[10] The resonance offset (see Fig. 4) introduces a modulation of the transient signals in Fig. 3. However, it is the envelope of the wiggles which constitutes the diffraction signal.

We see from Eq. (15) that the inverse Fourier transform of $S(\vec{p})$ yields the spatial distribution function $\rho(\vec{r})$. The spatial distribution function $\rho(z)$ obtained by Fourier transforming the data shown in Figs. 3(b) and 3(c) is presented in Figs. 4(b) and 4(c), and indicates clear resolution of the plate assemblies. The mean spacings of the plates were 1.8 ± 0.2 mm for the three-layer sample and 1.06 ± 0.10 mm for the five-layer sample;

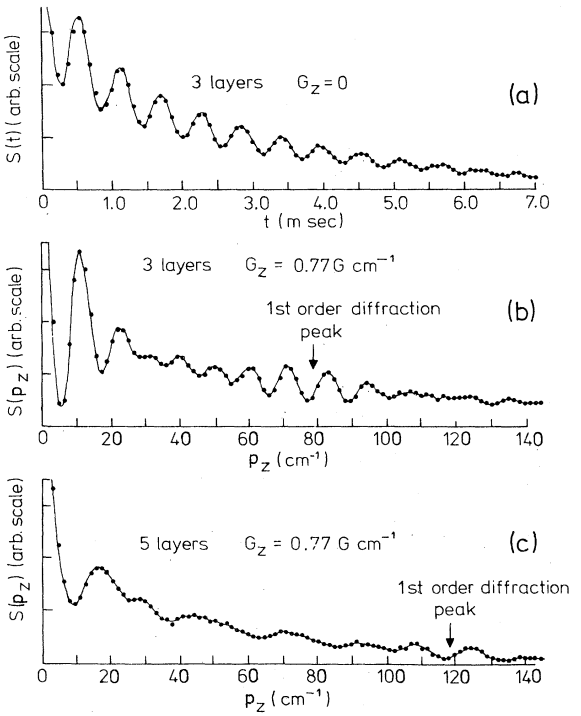

FIG. 3. (a) Transient nuclear signal from protons in a three-layer sample of synthetic camphor, $C_{10}H_{16}O$, in response to the $[\![1, 3, 2; 1, \bar{3}, 2]\!]$ multiple-pulse sequence, $\tau = 6.4$ μsec, with zero applied field gradient. (b) Same as (a) but with an applied field gradient of 0.77 G cm^{-1}. A first-order diffraction peak is observed. (c) Transient nuclear signal from protons in a five-layer sample of synthetic camphor in response to the same pulse sequence and the same field gradient as in (b). The abscissas in (b) and (c) were calculated from the measured values of the field gradient, and the multiple-pulse-sequence scaling factor, which was 2.1. The data were recorded off-resonance (see text and Fig. 4, and, also Ref. 10).

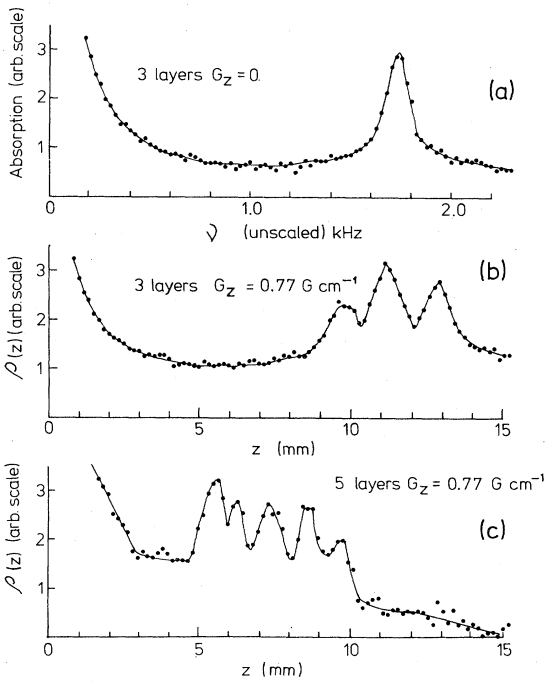

FIG. 4. (a) Fourier cosine transform of the transient response, Fig. 1(a). A narrowed linewidth of 150 Hz is observed. (b) Fourier cosine transform of the transient response, Fig. 1(b). The three camphor layers are clearly resolved. (c) Fourier cosine transform of the transient response, Fig. 1(c). The five camphor layers are well resolved. The abscissas in (b) and (c) were calculated from the measured values of the field gradient and the multiple-pulse-sequence scaling factor, which was 2.1. The peaks observed at the frequency origin arise from the damping and baseline shifts in the transient responses in Fig. 1.

these values are consistent with the spacings derived from Figs. 4(b) and 4(c) to within the 10% accuracy of our field-gradient calibration.[6]

2. *Liquids*

We have also obtained diffraction results for layered liquid samples and liquidlike rubber samples in response to a single 90° pulse at 15.0 MHz. Figure 5 shows the nuclear transient response from protons in a model one-dimensional lattice comprising seven layers of "Vaseline" petroleum jelly of mean thickness 0.54 mm and mean spacing 0.96 mm. The lifetime of the response without the linear gradient applied is limited mainly by the inhomogeneity of the static magnetic field. When a field gradient of 1.4 G cm^{-1} is applied, peaks in the response corresponding to first- and second-order diffraction can be seen. The decay of the first- and second-order diffraction peaks is somewhat faster than expected and is attributed in part to deviations from uniformity in the field-gradient coils.[17] Figure 6 is the theoretical expression Eq. (17) for a seven-layer sample with dimensions corresponding to the sample of Fig. 5. The positions of the first- and second-order diffraction peaks agree well with those observed in Fig. 5. The theoretical amplitudes should be further reduced by the intrinsic lifetime (see Fig. 5), but will still be substantially larger than observed experimentally, for reasons mentioned above.

IV. DISORDERED MATERIALS

In this section, we wish to consider the diffraction pattern and its spatial Fourier transform

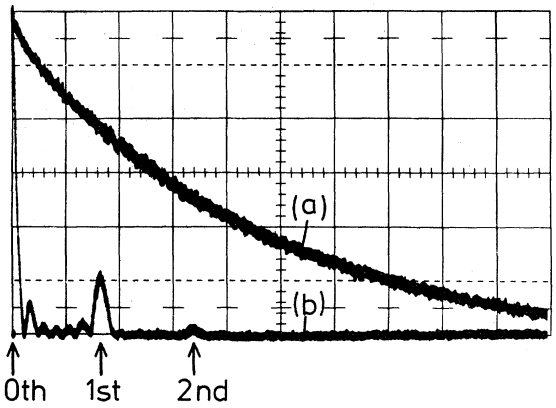

FIG. 5. (a) Nuclear transient response from protons in a model one-dimensional lattice comprising seven layers of "Vaseline" of mean thickness 0.54 mm and mean spacing 0.96 mm recorded at 15 MHz. The lifetime of the response is limited mainly by the inhomogeneity of the static magnetic field. (b) Nuclear transient response from the same sample when a magnetic field gradient of 1.4 $G\,cm^{-1}$ is applied. The labeled peaks in this response correspond to zeroth, first, and second orders of diffraction. Diode demodulation is employed. Time scale: 1 msec per large division.

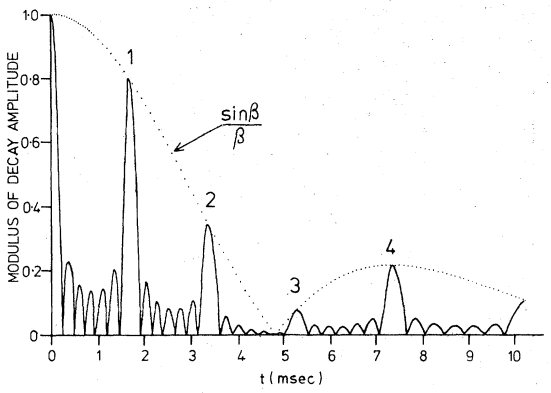

FIG. 6. Plot of the modulus of the theoretical expression, Eq. (17), for a model one-dimensional lattice with dimensions corresponding to the sample of Fig. 5. The zeroth-, first-, etc., order diffraction peaks are labeled 0, 1, 2, etc. The positions of the first- and second-order diffraction peaks agree well with the experimental data in Fig. 5.

when we have a partially disordered lattice. We are thinking particularly of systems like biological membranes, fibrous structures, or mosaic crystals, whose over-all spatial distribution may not be perfectly ordered. The question is, therefore, whether one expects to see an NMR diffraction signal in this case. Of course, x-ray studies in liquids and amorphous solids do in general reveal some structure, the origin of which was first explained by Zernike and Prins.[18] Their idea and subsequent developments in x-ray studies have allowed the so-called "radial distribution function" to be measured in liquids and amorphous solids.[19]

A. Model system

We consider a random collection of spheres of resonant nuclei with constant spin density ρ_0 confined within a rectangular container of dimensions J, K, L, where the direction of L coincides with that of the linear field gradient, which is applied along the z axis.

We shall approximate the spatial distribution function of the spheres $F(x, y, z)$ by

$$F(x, y, z) \simeq f(xy)g(z), \tag{20}$$

where $g(z)$ is a linear distribution which may be easily calculated. In performing the calculation, however, we shall further assume that the total number of spheres to be distributed along z is constant and therefore independent of x and y.

Thus, we imagine our random system to consist of a randomly spaced array $f(x, y)$ of M lines of N spheres, the spheres on each line being randomly distributed along its length.

If the mean spacing between sphere centers is greater than $2\sqrt{3}a$, where a is the sphere radius, we shall assume that there is no correlation between adjacent lines of spheres. We then refer to this case as the uncorrelated model, Fig. 7(a). If, however, the mean spacing is less than $2\sqrt{3}a$, then we would expect some correlation between adjacent lines of spheres from purely geometrical considerations. Indeed, in the perfectly interlocked, regular case, the spheres would form a

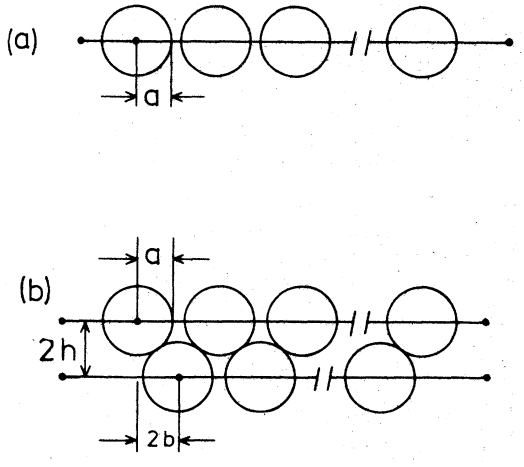

FIG. 7. Model linear distributions of spheres. (a) Uncorrelated model. (b) Correlated or interlocking model.

hexagonal-close-packed array.

We shall consider in particular the situation where the spheres are not quite touching; even in this case there can exist a highly ordered situation, as we shall see later. We shall also consider slight disordering of this regular case. This situation we shall approximate by the correlated model [Fig. 7(b)], bearing in mind that the aim here is to account only for minor deviations from the ordered state.

B. Linear distribution function

The analysis in this section follows closely the work of Zernike and Prins.[18] Consider a long row of adjacent cells of length Δz. Let some of the cells be occupied randomly, each with an occupation probability

$$p = \Delta z / l , \tag{21}$$

where l is the mean spacing between occupied cells.

The probability that m of the first n cells are occupied is, from probability theory,[20]

$$P_m(n) = \frac{n!}{m!(n-m)!} \frac{\Delta z^m}{l^m} \left(1 - \frac{\Delta z}{l}\right)^{n-m} , \tag{22}$$

which, in the limit $\Delta z \to 0$ with $n\Delta z = z'$ remaining finite, becomes the continuous function

$$P_m(z') = \frac{z'^m}{m! l^m} e^{-z'/l} . \tag{23}$$

This is the probability that m occupation sites will lie within the distance z'. To account for the finite radius a of our spheres and the fact that spheres cannot interchange along a row, we make the transformation in Eq. (23)

$$z = z' + (2m+1)a , \tag{24}$$

giving the linear distribution function for sphere *centers*,

$$g(z') = \left(e^{-(z-a)/l} + \frac{(z-2a)}{l} e^{-(z-3a)/l} + \frac{(z-3a)^2}{2l^2} e^{-(z-5a)/l} + \cdots \right) \Big/ l$$

$$= \sum_m g_m(z - (2m+1)a) , \tag{25}$$

where

$$g_m(z - (2m+1)a) = 0 \quad \text{for } z < (2m+1)a . \tag{26}$$

Equations (24)–(26) apply to the uncorrelated model. For the correlated model, we replace the transformation Eq. (24) by

$$z = z' + a + 2mb , \tag{27}$$

where

$$2b = 2(a^2 - h^2)^{1/2} \tag{28}$$

is the projected distance between the centers of touching spheres along the z axis [see Fig. 7(b)], and $2h$ is the distance between adjacent interlocking rows.

C. Diffraction signal

Using the distribution function, Eqs. (25) and (26), we are now able to calculate the diffraction signal. This is obtained from Eq. (15) for the one-dimensional case.

The spin density for a single homogeneous set of spins in the shape of a sphere of radius a centered z' from the origin is

$$\rho_s(z' - z) = \rho_0 \pi [a^2 - (z - z')^2] \quad \text{for } z' - a < z < z' + a . \tag{29}$$

Outside these limits, $\rho_s(z' - z) = 0$. Thus, in a simple generalization of Eq. (16), we obtain

$$S(p_z) = \mathrm{Re} \int_{-\infty}^{+\infty} \sum_m \rho_m(z) e^{ip_z z} dz , \tag{30}$$

where

$$\rho_m(z) = \int_{-\infty}^{+\infty} g_m(z' - a - 2mb) \rho_s(z' - z)\, dz' . \tag{31}$$

Since the full density distribution is observed experimentally, we shall need to calculate

$$\rho(z) = \sum_m \rho_m(z) . \tag{32}$$

1. Spin density distribution

For a completely random distribution with no order (corresponding to large l), we may replace the distribution function $g(z)$ by the step function $\Theta(z - a)/l$, in which case we obtain

$$\rho(z) = \begin{cases} \rho_0 \pi \{a^2 z - \frac{1}{3}[a^3 - (a - z)^3]\}/l & \\ \qquad \text{for } 0 < z \leq 2a , & \text{(33a)} \\ \frac{4}{3} \rho_0 \pi a^3 / l \quad \text{for } z > 2a . & \text{(33b)} \end{cases}$$

In calculating the density distribution in the general case, since the various functions occurring in Eq. (23) are discontinuous, the limits of integration and the corresponding ranges of z are important. For the first term in Eq. (25) corresponding to $m = 0$, we get

$$\rho_0(z) = \begin{cases} \int_a^{a+z} g_0(z' - a) \rho_s(z' - z) dz' & \\ \qquad \text{for } 0 < z < 2a & \text{(34a)} \\ \int_{z-a}^{z+a} g_0(z' - a) \rho_s(z' - z) dz' & \\ \qquad \text{for } z > 2a . & \text{(34b)} \end{cases}$$

For $m=1$, we obtain

$$\rho_1(z)=\begin{cases}\displaystyle\int_{a+2b}^{z+a+2b} g_1(z'-a-2b)\rho_s(z-z')dz' \\ \qquad\qquad \text{for } 2b<z<2(a+b) \quad (35a)\\ \displaystyle\int_{z-a}^{z+a} g_1(z'-a-2b)\rho_s(z-z')dz' \\ \qquad\qquad \text{for } z>2(a+b). \quad (35b)\end{cases}$$

These integrals have been calculated exactly up to $m=2$ and evaluated numerically for the particular cases discussed in Sec. IV D.

D. Experimental results

In order to test the predictions of the theory on a disordered material, model systems were constructed using spherical glass beads of 1.96-mm mean diameter with standard deviation of 0.02 mm. The complementary resonance signal was observed by surrounding the spheres with water. The signal from a distribution of spheres of spins may then be deduced using Babinet's principle.

The spheres plus water were contained in a square-cross-section glass cell, Fig. 8. The external cell dimensions were 10 mm square by 20 mm long. The receiver coil was a close fit around the cell and extended 10 mm along the length. The sample was oriented so that the field gradient G_z was normal to one face. In this case, for a homogeneous distribution of spins (i.e., no spheres), the absorption line shape was rectangular, Fig. 9.

1. Correlated model

For this case, the beads were first placed in the dry sample cell, then water was added. The cell was then ultrasonically agitated and occluded air was pumped off. The agitation also had the effect of ordering the spheres, giving the experimental density distribution shown in Fig. 10(a). Slight disordering of the spheres was achieved by giving the cell a single shake, which resulted in the density distribution of Fig. 10(b).

The complementary signals, corresponding to resonant spheres, are plotted in Fig. 11 and compared with the theoretical spin density Eq. (32), and indicate moderate agreement with the model.

2. Uncorrelated model

Since the beads need to be spaced apart by about one diameter, it was necessary to support the large beads by a solid matrix of 470-μm beads. As the smaller beads are on the threshold of the spatial resolution of the spectrometer, they did not affect significantly the signals observed.

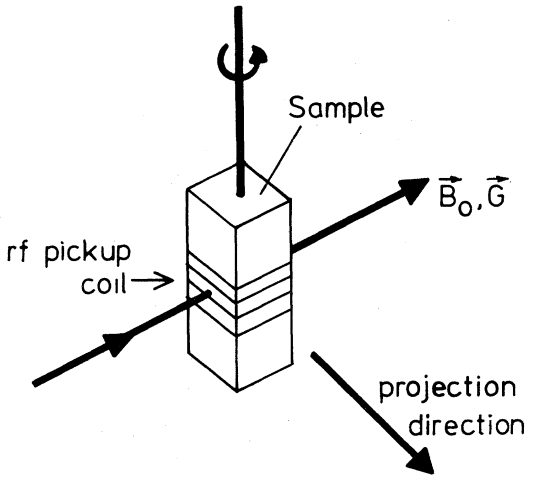

FIG. 8. Diagram showing rectangular sample and receiver coil geometry.

The samples were prepared as follows: A specified number of large beads and an arbitrary quantity of the 470-μm beads were placed in the sample cell and vigorously shaken to thoroughly mix them. Water was added slowly to just cover the beads. The cell was ultrasonically agitated and excess air was pumped off, allowing the beads to settle or bed down. The level of the beads was marked. After the experiment, the volume occupied by the beads was measured by filling the empty cell up to the mark with water. The volume of water was

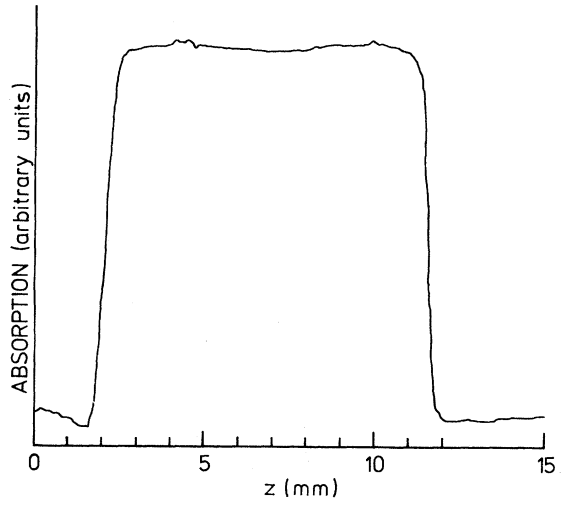

FIG. 9. Absorption line shape from protons in water contained in a glass sample cell of square crosssection. A linear magnetic field gradient of 1.42 G cm^{-1} is applied as indicated in Fig. 8. The center frequency is 15 MHz. The abscissas were determined from the measured field gradient.

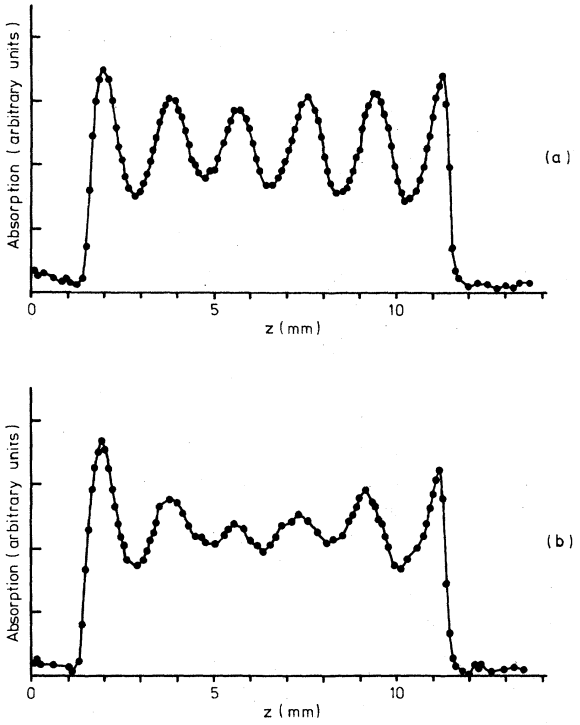

FIG. 10. (a) Absorption spectrum from well-ordered glass spheres immersed in water and contained in a cell of square cross section. The spectrum was obtained by Fourier transformation of the proton FID recorded at 15 MHz in a field gradient of 1.48 G cm^{-1}. The abscissas were derived from calibration of the field gradient. (b) As for (a) after the spheres have been slightly disordered by shaking.

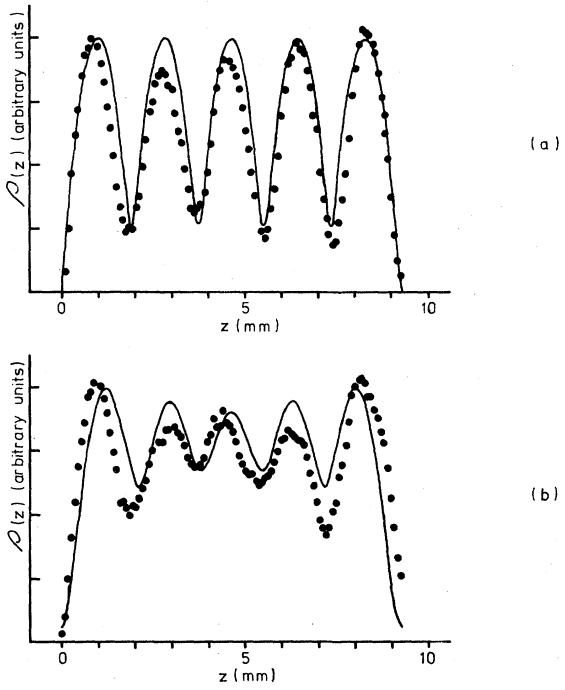

FIG. 11. The circles are the experimental spin densities for distributions of spheres of nuclei obtained by Babinet's principle from Fig. 10. The curves are Eq. 32 with $m=0$, 1, 2, reflected about $z=\frac{1}{2}L$ for convenience. (a) The curve corresponds to $N+1=5$, $a=0.98$ mm, $L=105$ mm, and $b=0.91$ mm, so that $l=0$. (b) This curve has $N+1=5$, $a=0.98$ mm, $L=105$ mm, and $b=0.75$ mm, so that $l=0.26$ mm, corresponding to some disorder, hence the damping.

deduced by weighing.

The density distribution results for 45 spheres in a volume of 1.62 cm^3 are shown in Fig. 12(a), while the result for 46 spheres in a 1.98 cm^3 volume is shown in Fig. 12(b). Again using Babinet's principle, the complementary signals are plotted in Fig. 13 and compared with the theoretical expression, Eq. (32), with $b=a$, giving fair agreement.

V. PRACTICAL AND THEORETICAL LIMITS TO SPATIAL RESOLUTION

In this section we examine quantitatively the principal limitations of NMR diffraction and discuss the factors affecting the spatial resolution obtainable. In both solids and liquids, the resolution is directly related to the uniformity of both the static magnetic field $\vec{B}_0$ and the applied linear field gradient $\vec{G}$. The intrinsic lifetime of the signal, T_2 or T_{2e} for multiple-pulse experiments, as well as translational diffusion, also play important roles.

For high resolution, chemical-shift variations and changes of the bulk electronic susceptibility will clearly have an important effect as well. The fact that spatial resolution depends on position in the field gradient implies that movements of both sample and gradient coil will be important.

Finally, the texture of the sample material itself and the presence of polycrystals will impose some limitations. We shall discuss the various factors in turn.

A. Resolution criteria

The criteria adopted for the just-resolved first-order diffraction peak of a one-dimensional lattice of spacing c are clearly arbitrary. However, they must depend on the signal-to-noise ratio of the initial signal in zeroth order. If R_0 is the initial signal-to-noise ratio and $R_{\min}$ is the minimum signal-to-noise ratio tolerable, we find from Eq. (16) that the time to the first diffraction peak ($g=1$) gives

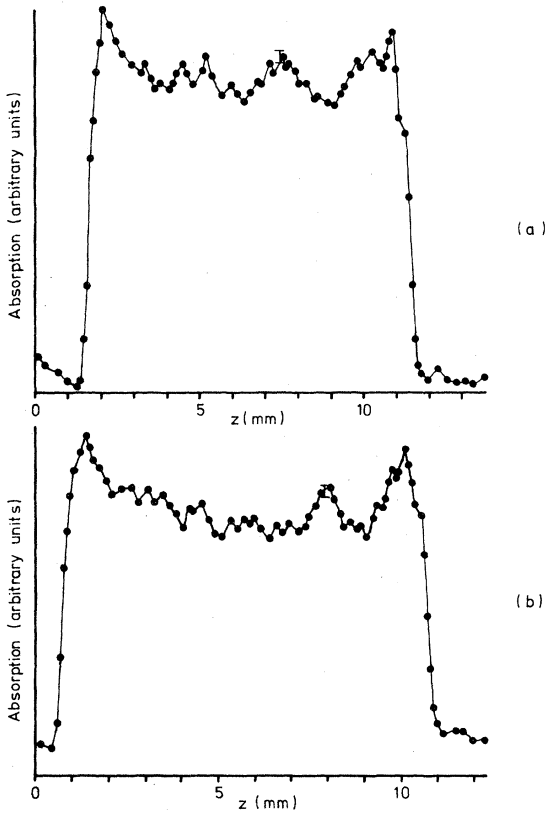

FIG. 12. (a) Absorption spectrum from 45 1.96-mm-diam glass spheres randomly distributed in a volume of 1.62 cm^3 supported in a matrix of 470-μm-diam spheres immersed in water and contained in a cell of square cross section. The spectrum was obtained by Fourier transformation of the proton FID recorded at 15 MHz with a field gradient of 1.33 $G\,cm^{-1}$. (b) As for (a) with 46 large spheres randomly distributed in 1.98 cm^3 and a field gradient of 1.48 $G\,cm^{-1}$. The abscissas were obtained from calibration of the field gradient.

$$t_1 = 2\pi/\gamma c\, G_z = T_{2\,\mathrm{eff}} \ln(R_0/R_{\min}) = \alpha T_{2\,\mathrm{eff}}\,, \qquad (36)$$

where $T_{2\,\mathrm{eff}}$ is the effective transverse relaxation time due to all broadening mechanisms present. The Rayleigh resolution criterion corresponds to $\alpha = 3.53$ in Eq. (36) for a Lorentzian line, which in turn corresponds to a 10% drop in signal amplitude from maxima to minima in the spatial or frequency distribution.

Numerically similar resolution criteria may be defined for other line shapes. For example, the Rayleigh criterion corresponds to truncation at $e^{-3.26}$ for a Gaussian decay and $e^{-3.35}$ for an $\exp(-t^3)$ decay.

Evaluation of Eq. (36) will depend on the various magnetic fields available and the various line-broadening factors, which we now discuss in turn.

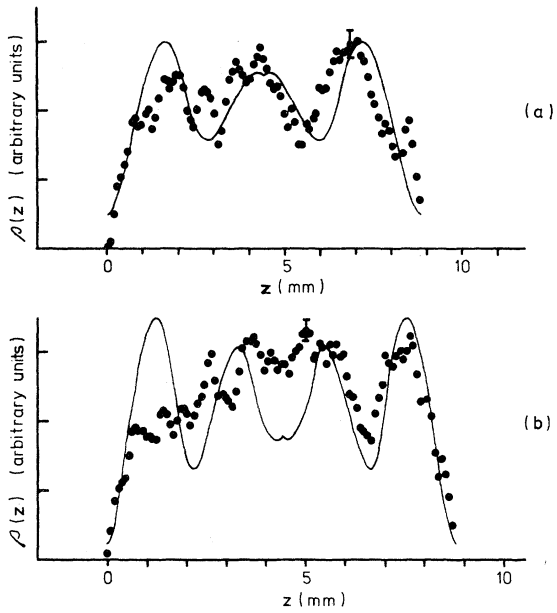

FIG. 13. The circles are the experimental spin densities for distributions of spheres of nuclei obtained from Fig. 12 by Babinet's principle. The curves are Eq. (32), with $m = 0$, 1, 2 and for $a = b$, and are reflected about $z = \frac{1}{2}L$ for convenience. (a) The curve corresponds to $N + 1 = 3$, $L = 88.2$ mm, and $a = 1.08$ mm, so that $l = 0.77$ mm. (b) The curve corresponds to $N + 1 = 3$, $L = 87.0$ mm, and $a = 0.88$ mm, so that $l = 0.42$ mm.

1. Line-broadening factors

a. Static field. If $f = \Delta B/B_0$ is the fractional static-field inhomogeneity over the sample, $\Delta\chi$ is the inhomogeneity of the bulk susceptibility over the sample due, perhaps, to macroscopic regions of different susceptibility, and if $\langle \delta^2 \rangle^{1/2}$ is the average chemical-shift variation over the sample, then the effective linewidth due to these terms treated as independent Lorentzian lines is

$$\Delta W_{\mathrm{field}} = \gamma B_0 (f + \Delta\chi + \langle \delta^2 \rangle^{1/2}). \qquad (37)$$

b. Structural inhomogeneity. In a regular structure, small deviations and imperfections over the bulk sample, attributable to a polycrystal mosaic structure or other causes, will give a line broadening

$$\Delta W_{\mathrm{struct}} = \langle \Delta z^2 \rangle^{1/2} G_z\,, \qquad (38)$$

where $\langle \Delta z^2 \rangle^{1/2}$ is an average spatial deviation. This term can also contribute if the sample moves during, for example, a multishot signal-averaging process. That is to say, such movements may not affect the resolution directly in individual shots but rather in a collective manner, through signal averaging.

c. Diffusion. The time for the transverse response to decay to e^{-1} of its initial value through translational self-diffusion of spins in a linear field gradient G_z is[7,15]

$$T_{2\,\mathrm{diff}} = (3/D\gamma^2 G_z^2)^{1/3}, \tag{39}$$

where D is the self-diffusion constant. This gives a linewidth contribution ΔW_{diff} which depends rather on the line shapes of the various other contributed terms. In general, all the factors affecting the linewidth produce different line shapes, so the over-all linewidth can only be specified generally in functional form:

$$\Delta W_{\mathrm{tot}} = f(\Delta W_{\mathrm{field}}, \Delta W_{\mathrm{struct}}, \Delta W_{\mathrm{diff}}, \Delta W_{\mathrm{int}}). \tag{40}$$

Here, the intrinsic linewidth contribution $\Delta W_{\mathrm{int}} = 1/\pi T_{2\,\mathrm{int}}$, and the intrinsic transverse-decay-time constant $T_{2\,\mathrm{int}} = T_{2\epsilon}$ for multiple-pulse sequences, while for single-pulse experiments in liquids, $T_{2\,\mathrm{int}} = T_2$.

2. Field gradient uniformity

A practical coil configuration designed to produce a uniform gradient G_z will in general produce small undesirable gradients ΔG_x and ΔG_y in some regions of the sample which we shall label collectively as ΔG. If we wish to resolve a distance Δz in a total sample volume L^3, then we must satisfy the condition

$$\Delta G/G_z = \Delta z/L. \tag{41}$$

For over-all optimal conditions, we would take Δz as the smallest resolvable distance caused by all factors *other* than the linear-gradient coils. This distance is of course related to the linewidth by

$$\Delta W_{\mathrm{tot}}/G_z = \Delta z. \tag{42}$$

Taken together, Eqs. (41) and (42) mean that when $\Delta W_{\mathrm{tot}} = \gamma f B_0$ and $B_0 > G_z L$, the required fractional nonuniformity in the field gradient can be less than that required of the static field.

The *linearity* of the z gradient will not in general affect the resolution, since all spins in the xy plane are isochromatic. It would, of course, affect the linearity of the Fourier transform and, if uncorrected, would give compression of the axes.

B. Practical resolution

1. Solids

Let us assume that $\alpha = 3$ in Eq. (36). In current multiple-pulse sequences, the line narrowing achieved is adversely affected by resonance offset.[11,16] A conservative value for the multiple-pulse decay-time constant $T_{2\epsilon}$ is 2.0 msec for protons, and in order to keep within this value, the total static-field variation across the sample should not exceed about 1 G.[11] For a sample 0.1 mm thick, this corresponds to a maximum field gradient $G_z = 100$ G cm^{-1}. This is a fairly modest gradient and should be easily achieved by conventional means.[17,21] If $T_{2\epsilon}$ is the only broadening source, then the best spatial resolution obtainable for protons in a solid is ~4.0 μm. In fact, as discussed in Sec. III A, the $\Delta W_{\mathrm{field}}$-broadening contributions can in principle be removed by using a specially designed multiple-pulse sequence. However, for protons in solids at low frequencies, that is, 10–20 MHz, chemical shifts should not be a worry.

The gradient uniformity required in the above example is, from Eq. (41), only 4.0%. A lower limit for the diffusion constant may be estimated by taking the diffusion contribution to the decay-time constant to be at least $10T_{2\epsilon} = 20.0$ msec. This assures negligible additional diffusional broadening. For $G = 100$ G cm^{-1}, this gives $D = 6 \times 10^{-8}$ cm^2 sec^{-1}. Many solids have diffusion constants much smaller than this at room temperature. For example, in ice at 273 °K, $D = 3 \times 10^{-11}$ cm^2 sec^{-1}; in adamantane at 300 °K, $D = 10^{-21}$ cm^2 sec^{-1}.[22] Of course, for a sample as thin as 0.1 mm, it may be necessary to enhance the signal-to-noise ratio by lowering the temperature. In this case, the diffusion constant will become even smaller.

It is clear that for most solids the spatial resolution is currently limited by the line narrowing achieved in the multiple-pulse sequence. Fundamental limits due to diffusion alone ($D = 10^{-21}$–10^{-17} cm^2 sec^{-1}) would correspond to $c = 2$–5 Å. The gradient uniformity required in the diffusion-limited case would have to be 5 parts in 10^6!

2. Liquids

In liquids the major limitations to resolution are likely to be static-field inhomogeneity and diffusion. It turns out that the Rayleigh criterion with Eq. (39) is equivalent to allowing the spins to diffuse an average distance about equal to the spatial resolution desired. If one works with a single 90° excitation pulse, static-field inhomogeneity effects and chemical shift would remain and could present problems at high static fields. Of course, one could use multiple-pulse and switched-gradient methods here as well. However, the problem can be avoided by working at lower static fields.

If we take diffusion as the limiting mechanism of resolution, and consider protons in water in particular as the material most common in, for example, biological specimens, then for $D = 1.85 \times 10^{-5}$ cm^2 sec^{-1} and $G = 100$ G cm^{-1}, we find a resolution limit of 6 μm. Since the water must remain liquid, diffusion is not an experimental

variable, so that resolution improvements must come from larger field gradients. It is of interest to consider the size of the gradient required to resolve 5 Å in water. Its value must be $G_z = 1.5 \times 10^{14}$ Gcm^{-1}, with a corresponding uniformity of 5 parts per million.

Of course, in liquid experiments using one 90° pulse, we are no longer constrained to keeping the magnetic field span across the sample down to 1 G as for solids. This allows larger samples to be used.

VI. NMR MICROSCOPY

We have already shown in Eq. (15) that the spin-density distribution $\rho(\vec{r})$ may in general be obtained from $S(\vec{p})$ by taking the inverse Fourier transform. The one-dimensional Fourier transform is straightforward to perform and may be useful if the general form of the object is known. Figure 14 illustrates this point. It is a sketch showing the expected lineshape for a cylinder of spins in a field gradient as indicated.[23,24]

Some experimental results for various samples are presented in Fig. 15. Figure 15(a) is the proton-spin distribution for a cylinder of water 13.4 mm in diameter, while Fig. 15(b) is the spin distribution for the same object but with a coaxial occlusion 9.8 mm in diameter containing no spins. The axes of these distributions are transverse to the cylindrical axis in each case, as indicated in Fig. 14. The distributions shown are characteristic of this sample geometry. The spatial resolution achieved here is about 0.5 mm, and is limited by the nonuniformity of the field gradient.[17]

Figures 15(c) and 15(d) are one-dimensional spin-density distributions of the tip of the left-hand little finger of P. K. G. recorded *in vivo*.[25] Strong proton signals are received from the skin, subcutaneous tissues, synovial sheath, blood vessels, etc., while much weaker signals come from the distal phalanx. The NMR coil was positioned over the region where the nail merges with the eponychium. The general similarity between Fig. 15(b) and Figs. 15(c) and 15(d) is consistent with the fingertip being approximately cylindrical with the bone centrally placed. Also apparent in Figs. 15(c) and 15(d) is a small distortion caused by the nail.

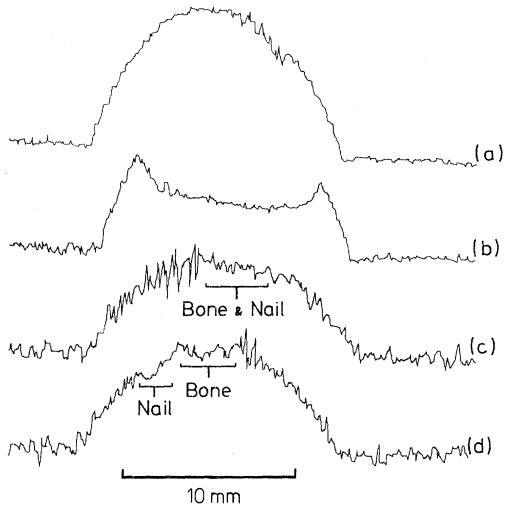

FIG. 15. One-dimensional projections obtained by NMR microscopy. In each case, the NMR sample coil was 18 mm in diameter and 3 mm deep. The scale indicated was obtained from calibration of the gradient. (a) Projection of a cylinder of water 13.4 mm in diameter. (b) Projection of a cylinder of water 13.4 mm in diameter with a coaxial proton-free occlusion 9.8 mm in diameter. (c) Projection of the left-hand little finger of P. K. G. The lunule of the nail was positioned under the NMR coil. (d) As for (c), with the digit rotated through approximately 45°. The left-hand side of the spectrum corresponds to the dorsal surface of the digit.

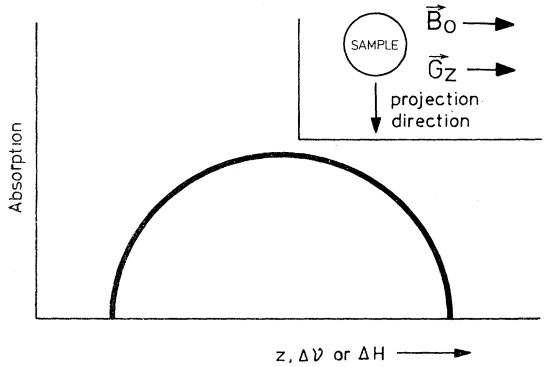

FIG. 14. Diagram showing the expected line shape for a cylindrical sample of spins with uniform density, placed in a uniform magnetic field gradient. The inset shows the field-gradient direction which is normal to the projection direction.

Full three-dimensional Fourier transforms, though difficult to perform unambiguously, would be extremely valuable, since one would then have the full three-dimensional structure of the object. In two dimensions, $\rho(x, y)$ represents a cross-sectional picture or micrograph of the object. We now consider the theory of such reconstructions.

A. General theory

If we consider a general two-dimensional object consisting of a continuous spin-density distribution

$\rho(\vec{r})$, divided into a regular array by a grid with lattice spacings a, b, and with a continuous density distribution within grid cells, then the transverse response signal is, from Eqs. (15) and (16),

$$S = \mathrm{Re} \sum_l \sum_m \exp[2\pi i(le+mf)]\rho_{lm}, \tag{43}$$

where ρ_{lm} is an integrated spin density for the l,mth matrix element. If we now set

$$le+mf = Ph, \tag{44}$$

P integer, with $h = dG\gamma t/2\pi$ and d the projected lattice constant, Eq. (43) can be regrouped to give

$$S = \mathrm{Re} \sum_P e^{2\pi iPh}\rho_P, \tag{45}$$

where

$$\rho_P = \sum_{l,m} \rho_{lm}, \tag{46}$$

subject to P being constant. The inverse Fourier transform of Eq. (45) produces ρ_P which, as we see from Eqs. (44) and (46), is just the Pth projection of the total matrix ρ. ("Projection" here is used in the sense of the optical analogy, where the passage of a parallel beam through an opaque material produces a shadow or projection the intensity of which depends on the integrated optical density along the beam path.) A similar result pertains for three dimensions and, in this case, $\rho_P = \sum_{l,m,n} \rho_{lmn}$, where $Ph = le+mf+ng$.

The grid spacings are arbitrary and control the resolution of the spin-density map or micrograph. In the present work we shall take $a = b$ and $l = m$, that is, a square array. The problem is, therefore, equipped with the various projections ρ_P corresponding to various directions, how do we reconstruct the density map? We shall restrict our present discussion to two-dimensional arrays for simplicity.

B. Image reconstruction

The problem of reconstructing an image from its projections is an old one motivated by the need to reconstruct two- and three-dimensional images from electron micrographs, x-ray shadowgraphs, and one-dimensional scans of cosmic distributions.[26-31]

In x-ray and electron-microscopy studies, the need to reconstruct images from a few projections has arisen because of the radiation damage produced in the sample. In NMR microscopy, damage of the specimen presents a much smaller hazard.[25] However, in physiological applications, it is important to produce micrographs rapidly and simply. For this reason we describe our simple procedure.

1. General method

For a square matrix ρ of discrete points ρ_{lm}, reconstruction from the projections is straightforward. For an $m \times m$ array, there are m^2 unknowns. Along the [10] direction there are m projections and, crudely speaking, if we look at the object in m directions, we have m^2 equations which may be solved simultaneously to give a unique determination for all points ρ_{lm}. In practice, one does not have to solve the complete set of equations simultaneously. Referring to Fig. 16, ρ_{11} can be determined directly for all projection directions greater than [10], that is to say, [11], [12], etc. Having determined this point, ρ_{12} can likewise be determined from the [12] projection direction. Once suitable single elements have thus been determined, they can then be used in combination to determine other points, possibly with lower-order projection directions. For example, given ρ_{12}, then ρ_{21} may be determined from the [11] projection direction. This procedure is *exact* and therefore unambiguous for a point matrix or for elements whose extent do not cause overlap with other elements which are not supposed to be contributing to the projection for a given direction. From this point of view, neither the [10] nor [01] projection direction gives overlap troubles. The higher-order projection directions do, however, give overlap troubles, which are not necessarily ameliorated by reducing the grid size. A particular array ele-

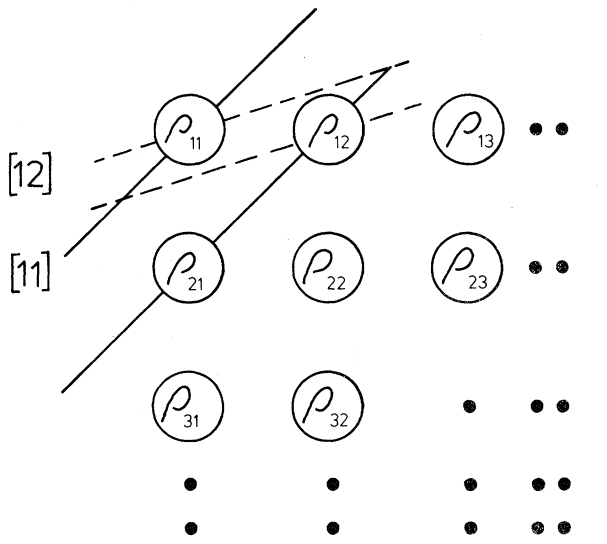

FIG. 16. Sketch of a two-dimensional discrete-density distribution showing two projection directions. Note that ρ_{11} may be determined from either the [11] or [12] projection direction, whereas ρ_{12} may be determined uniquely from [12] only.

ment will show variation when determined independently from a number of projections in a continuous array. In this case we take the average, $\bar{\rho}_{lm}$, but this leads automatically to none of the projections being quite satisfied. In spite of this difficulty, image reconstruction using this method does give a recognizable micrograph.[32]

C. Results and discussion

Figure 17 is a simple two-dimensional image obtained using the method outlined here, by combining the results of five spin-density projections identical to Fig. 15(b) for rotations about the cylindrical axis. The reconstruction is based on a 17×17 matrix using ten gray levels. The calculations were done by hand. Despite the coarseness resulting from the relatively small number of matrix elements, the image shows the broad features to be expected, viz., a proton-dense annulus enclosing a circular proton-free occlusion.

Another approach to spin-density mapping for liquids, recently proposed by Hinshaw,[33] uses two or three sinusoidally time-varying magnetic field gradients which reduce the isochromatic plane to a line or a point, respectively. Data acquisition could take considerably longer by this method for equivalent resolution and signal-to-noise ratio. We therefore briefly consider the analysis of the relative data-acquisition times of the two imaging methods.

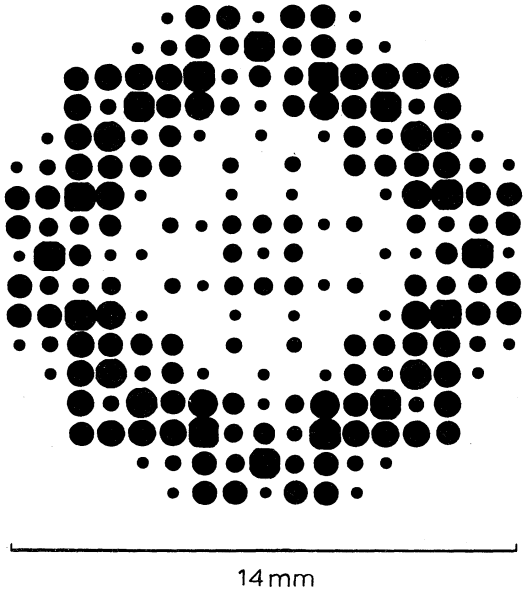

FIG. 17. Two-dimensional image reconstructed from five projections from data similar to Fig. 15(b), using the method outlined in Sec. VI B 1. Each projection was digitized using ten gray levels, and the reconstruction was based on a 17×17 matrix. The proton density in the image is depicted by dots of various diameters. The false proton density at the center of the image is a noise-introduced artifact produced by the matrix-reconstruction technique.

If we consider a micrograph of m^2 elements and take the time to record the data from one transient decay as $(t_d)_p$ for the projection method and $(t_d)_m$ for mapping method, the time to acquire the data for m projections by the projection method is

$$T_p = m(t_d)_p + t_{pp}\,, \tag{47}$$

whereas for the point-mapping method the time is

$$T_m = m^2(t_d)_m + t_{pm}\,, \tag{48}$$

where t_{pp} and t_{pm} are the data-processing times for the projection and mapping methods, respectively. For regular pulsing, we may take $(t_d)_p = (t_d)_m = \alpha T_1$, where T_1 is the mean spin-lattice relaxation time and α is a positive scaling factor. Let $\Delta W_m = 2\pi/T_{2m}$ and $\Delta W_p = 2\pi/T_{2p}$ be the respective bandwidths over which signal is received, and T_{2m}, T_{2p} the corresponding inhomogeneous transverse decay times.

Let S_0 be the single-shot signal arising from the entire sample and N_0 the noise corresponding to the bandwidth ΔW_p. The signal-to-noise ratio of a point defined over the frequency range ΔW_m relative to the frequency range $\Delta W_p = 2m\Delta W_m$, is therefore,

$$\left(\frac{S}{N}\right)_m = \frac{S_0}{m^2 N_0}\left(\frac{\Delta W_p}{\Delta W_m}\right)^{1/2} = \left(\frac{S}{N}\right)_p (2m)^{1/2}\,. \tag{49}$$

To achieve the *same* signal-to-noise ratio in the projection method, the signal must be sampled $2m$ times.[34] Since $2m\,T_{2p} = T_{2m}$, this may clearly be achieved in the time $(t_d)_p$ by recalling and sampling the signal in a Carr-Purcell echo sequence.[7] In this analysis, we assume that no further signal-to-noise enhancement by echo methods is possible in the point-mapping method due to the time dependence of the field gradients.

If $m(t_d)_m \gg t_{pp}$, t_{pm}, the relative acquisition time becomes

$$T_m/T_p = m\,. \tag{50}$$

For large m, therefore, the projection method is superior from the point of view of data-output rate.

VII. CONCLUSIONS

The new technique of NMR diffraction and microscopy has been presented together with the appropriate analysis following optical analogies. It is shown that certain effects common in optics and x-ray diffraction have their counterpart in NMR diffraction. In particular, NMR of disordered systems in the region of a boundary can be made to

yield the spin-density distribution analogous to the radial distribution function in x-ray studies.

A critical account of the limits of spatial resolution expected in NMR diffraction and microscopy is given, and this shows that with a technologically reasonable field gradient of 100 $G cm^{-1}$, the best resolution obtainable in a liquid (water) is about 6 μm, the principal limit being translational self-diffusion. For solids, using multiple-pulse line-narrowing techniques, the resolution limit is currently 4 μm. In this case, however, the limit is imposed by the intrinsic linewidth due to imperfections in the multiple-pulse sequence used. For this reason, we believe that the practical realization of NMR diffraction and microscopy presents new and compelling reasons for continued efforts to improve the line-narrowing efficiencies of these sequences.

The problem of reconstructing the two-dimensional Fourier transform from its projections is also discussed. The two-dimensional image or micrograph allows examination of internal and external structures and characteristics of specimens. The application to biological materials is stressed and an example of its application to a physiological specimen *in vivo* is given.

Finally, we remark that an intriguing possibility may exist for the study of nuclear-spin–phonon interactions in solids placed in a linear magnetic field gradient. The passage of an acoustic plane wave through a solid (or even a liquid) should produce observable variations in the NMR diffraction pattern. Indeed, in a continuous and homogeneous material, formation of a standing wave might be made to produce a diffraction pattern in its own right. We hope to report on these possibilities elsewhere.

ACKNOWLEDGMENTS

We wish to thank A. N. Garroway and D. C. Stalker for their assistance in performing some of the early experiments presented in this paper, A. A. Maudsley for performing the reconstruction of Fig. 17, and C. J. Doran for implementing the reconstruction algorithm of Ref. 30.

---

*Work supported by an equipment grant from the Science Research Council.

†Imperial Chemical Industries Ltd., post-doctoral Fellow. Present address: Department of Physics, University of Keele, Staffordshire, ST5 5BG, England.

[1]P. Mansfield and P. K. Grannell, J. Phys. C 6, L422 (1973); Phys. Bull. Inst. Phys. Lond. 25, 134 (1974).

[2]P. Mansfield, P. K. Grannell, A. N. Garroway, and D. C. Stalker, in *Proceedings of the First Specialized Colloque Ampere*, edited by J. W. Hennel (Institute of Nuclear Physics, Krakow, 1973), p. 16.

[3]P. C. Lauterbur, Nature 242, 190 (1973).

[4]R. Gabillard, C. R. Acad. Sci. (Paris) 232, 1551 (1951); Phys. Rev. 85, 694 (1952). This work is summarized by E. R. Andrew in *Nuclear Magnetic Resonance* (Cambridge U. P., Cambridge, England, 1956), p. 135.

[5]R. Gabillard, Rev. Sci. 90, 307 (1952).

[6]R. Bradford, C. Clay, and E. Strick, Phys. Rev. 84, 157 (1951).

[7]H. Y. Carr and E. M. Purcell, Phys. Rev. 94, 630 (1954).

[8]E. R. Andrew, A. Finney, and P. Mansfield, Royal Radar Establishment Reports 1967–1970 (unpublished).

[9]J. S. Waugh, L. M. Huber, and U. Haeberlen, Phys. Rev. Lett. 20, 180 (1968).

[10]P. Mansfield, M. J. Orchard, D. C. Stalker, and K. H. B. Richards, Phys. Rev. B 7, 90 (1973).

[11]A. N. Garroway, P. Mansfield, and D. C. Stalker, Phys. Rev. 11, 121 (1975).

[12]P. Mansfield, Phys. Rev. 151, 199 (1966).

[13]L. P. Kadanoff and G. Baym, *Quantum Statistical Mechanics* (Benjamin, New York, 1962).

[14](a) T-Y Wu and T. Ohmura, *Quantum Theory of Scattering* (Prentice-Hall, Englewood Cliffs, N. J., 1962); (b) C. L. Andrews, *Optics of the Electromagnetic Spectrum* (Prentice-Hall, Englewood Cliffs, N. J., 1961).

[15]A. Abragam, *The Principles of Nuclear Magnetism* (Clarendon, Oxford, 1961).

[16]W-K Rhim, D. D. Elleman, and R. W. Vaughan, J. Chem. Phys. 59, 3740 (1973).

[17]J. E. Tanner, Rev. Sci. Instrum. 36, 1086 (1965). Our gradient coils, following Tanner's design, had minimum and maximum radii of 50.4 and 59.7 mm for the experiments at 9.0 MHz and 58.4–78.4 mm for the experiments at 15.0 MHz. The magnet gap at the lower frequency was 58.5 mm and 79.0 mm at the higher frequency.

[18]F. Zernike and J. A. Prins, Z. Phys. 41, 184 (1927).

[19]B. D. Cullity, *Elements of X-ray Diffraction* (Addison-Wesley, Reading, Mass., 1959).

[20]H. Margenau and G. M. Murphy, *The Mathematics of Physics and Chemistry* (Van Nostrand, Princeton, 1957).

[21]R. S. Parker, I. Zupančič, and J. Pirš, J. Phys. E 6, 899 (1973).

[22]H. A. Resing, Mol. Cryst. Liq. Cryst. 9, 101 (1969).

[23]J. S. Murday and R. M. Cotts, J. Chem. Phys. 48, 4938 (1968).

[24]J. S. Murday, J. Mag. Res. 10, 111 (1972).

[25]P. K. Grannell and P. Mansfield, Phys. Med. Biol. 20, 477 (1975).

[26]R. N. Bracewell and A. C. Riddle, Astrophys. J. 150, 427 (1967).

[27]B. K. Vainshtein, Sov. Phys.-Crystallogr. 15, 781 (1971).

[28]A. Klug and R. A. Crowther, Nature 233, 435 (1972).

[29]R. Gordon, R. Bender, and G. T. Herman, J. Theor. Biol. 29, 471 (1970).

[30]R. Gordon and G. T. Herman, Commun. Assoc. Comput. Mach. 14, 759 (1971).

[31]A. Rosenfeld, *Picture Processing by Computer* (Aca-

demic, New York, 1969).

[32]We have also tried the reconstruction algorithm of Gordon and Herman (Ref. 30) using four directions and the same data as for Fig. 17 of the text. Implemented strictly according to the description given in their paper, the second method seems incapable of producing an adequate reconstruction sufficiently quickly for practicable use on, for example, a Nova 1220 minicomputer. Particular difficulty was experienced when there was high contrast in the picture. However, their first and simpler algorithm does give a picture in a reasonable time. But since the method satisfies the various projections consecutively and *not* simultaneously, it is of less value.

[33]W. S. Hinshaw, Phys. Lett. A 48, 87 (1974).

[34]Possible additional noise averaging in the reconstruction of the image from its m projections is entirely ignored in this analysis.